Pharm Res (2014) 31:2975–2987
DOI 10.1007/s11095-014-1392-5

RESEARCH PAPER

New strategy to surface functionalization of polymeric nanoparticles: one-pot synthesis of scFv anti-LDL(−) -functionalized nanocapsules

Eduardo A. Bender • Marcela F. Cavalcante • Márcia D. Adorne • Letícia M. Colomé • Sílvia S. Guterres • Dulcinéia S. P. Abdalla • Adriana R. Pohlmann

Received: 24 January 2014 / Accepted: 15 April 2014 / Published online: 8 May 2014

ABSTRACT

Purpose In general, the surface functionalization of polymeric nanoparticles is carried out by covalently bounding ligands to the nanoparticle surface. This process can cause a lack or decrease of the ligand specificity to its target receptor, besides the need of purification steps. We proposed a ligand-metal-chitosan-lecithin complex as a new strategy to functionalize the surface of biodegradable nanoparticles.

Methods One pot synthesis of scFv anti-LDL(−)-functionalized nanocapsules was carried out by self-assembly and interfacial reactions. Particle sizing techniques, lipid peroxidation and molecular recognition by enzyme linked immuno sorbent assays were carried out.

Results The selected formulation had unimodal size distribution with mean diameter of about 130 nm. The metals in the complex did not enhance the oxidative stress, and the scFv anti-LDL(−)-functionalized nanocapsules recognized LDL(−) and did not react with native LDL indicating the maintenance of the active site of the fragment.

Conclusions The one pot synthesis, using the ligand-metal-chitosan-lecithin complex to functionalize the surface of the biodegradable nanocapsules, maintained the active site of the antibody fragment making the device interesting for applications in nanomedicine.

KEY WORDS LDL single-chain fragment variable · ligand-metal-chitosan-lecithin · lipid-core nanocapsules · polycaprolactone

ABBREVIATIONS

DLS	Dynamic light scattering
ELISA	Enzyme linked immuno sorbent assay
LD	Laser diffractometry
LDE	Laser Doppler electrophoresis
LDL	Low density lipoprotein
LDL(−)	Electronegative low density lipoprotein
LNC	Lipid-core nanocapsules
MCMN	Metal complex multi-wall nanocapsules
MDA	Malondialdehyde
MN	Multi-wall nanocapsules
nLDL	Native low density lipoprotein
NTA	Nanoparticle tracking analysis
PCL	Poly(ε-caprolactone)
PDI	Polydispersity index
Phe	Phenylalanine

Electronic supplementary material The online version of this article (doi:10.1007/s11095-014-1392-5) contains supplementary material, which is available to authorized users.

E. A. Bender • M. D. Adorne • L. M. Colomé • S. S. Guterres
Programa de Pós-Graduação em Ciências Farmacêuticas
Faculdade de Farmácia, Universidade Federal do Rio Grande do Sul Porto Alegre, RS, Brazil

M. F. Cavalcante • D. S. P. Abdalla
Faculdade de Ciências Farmacêuticas, Universidade de São Paulo
São Paulo, SP, Brazil

A. R. Pohlmann (✉)
Departamento de Química Orgânica and Programa de Pós-Graduação em Nanotecnologia Farmacêutica, Instituto de Química
Universidade Federal do Rio Grande do Sul, PBOX 15003,
Porto Alegre 91501-970, RS, Brazil
e-mail: pohlmann@iq.ufrgs.br

scFv anti-LDL(−)	Anti-electronegative LDL single-chain fragment variable
SPAN	Polydispersity
TBA	Thiobarbituric acid
TBARS	Thiobarbituric acid reactive substances
TEM	Transmission electron microscopy

INTRODUCTION

Nanotechnology has been impacting the development of new products in the past 20 years. Specifically in the field of human health, the evolution in nanomedicine has assumed an important role to improve therapy and diagnosis with potential applications in research, biomedicine or pharmaceutical and chemical industries (1–5). Different materials have been proposed to constitute the nanoparticles acting as drug delivery systems or diagnosis agents.

The use of nanoparticles for passive targeting based on the drug encapsulation, as well as for drug active targeting by nanoparticle surface functionalization and the use of nanoparticles suitable for *in vivo* monitoring have provided several advantages over methods traditionally employed (4–6). Among the main advantages of those nanoparticles, we can cite the development and/or improvement of diagnose or therapeutic methods, which provide better protection of drugs, nucleic acids, peptides, antibodies and other biomolecules, when compared to conventional approaches (7–9).

Different materials can be used to prepare nanoparticles such as ceramic, carbon nanotubes, organic polymers, lipids, metal oxides and metals. Nanomaterials (nanostructured materials) are in general formed by elements or organic molecules (1).

Among the biological applicability of metal nanostructures, their use to identify or combat microorganisms such as bacteria, fungi and viruses has been widely investigated (10). Furthermore, antibody-coated gold nanoparticles or other nanoparticles for viral detection as agents for images and for the development of immunodiagnostic kits have been described (5,11).

The active or passive targeting of nanoencapsulated drugs in the body depends on the physico-chemical characteristics of the nanocarriers rather than those of the drugs. Passive targeting is dependent of the distribution size, shape and wettability (hydrophilic surface) of the nanoparticles. Whereas, active targeting involve the use of site specific conjugates peripherally bound to the nanostructures, which allow the connections on particular sites in the body according to the specificity of the ligand with the target molecular system (4,6).

The nanoparticle surface functionalization with ligands, such as peptides, antibodies or antibody fragments is carried out primarily by conjugation methods (12). Those ligands are in general covalently bound either to the nanoparticle surface or to a linker molecule, such as poly(ethylene glycol) (6,13). Conjugation of the antibody can be random or site specific. Random conjugation can cause a lack of the ligand specificity, since the new chemical bond may occur exactly on the active site of the binding antigen. In this case, the ability of those particles to specifically binding to its target receptor might be decreased (4). On the other hand, a strategy of site specific binding assures full ligands activity. Besides, the one-pot syntheses of surface functionalized nanoparticles may constitute a versatile strategy to have different nanoparticles prepared with similar core-structures with a variety of ligands at their surface. The advantage of this strategy is the rapid and economic synthesis of surface-functionalized nanoparticles. Nevertheless, the challenge of that approach is to obtain the products in one-pot synthesis with no need of purification steps.

In the past few years, we developed two different structures: the lipid-core nanocapsules (14,15) and the spray-dried chitosan-metal microparticles (16). The former are nanocapsules containing a dispersion of caprylic/capric triglyceride and sorbitan monostearate, as core, poly(ε-caprolactone), as polymer hydrophobic wall, and polysorbate 80 micelles, as coating material to give the necessary wettability to prevent agglomeration of the nanoparticles in the aqueous phase. The latter structures are spray-dried microparticles of chitosan-metal complexes, which surface was cross-linked with glutaraldehyde. Earlier studies had investigated a metal complexation with chitin (chitosan precursor) by infrared and Mössbauer spectroscopy (17). The metal complex is formed as a chelate by coordinating with the oxygen and nitrogen atoms of the polysaccharide. Besides, recently we developed chitosan-coated lipid-core nanocapsules in aqueous turbid solution (18) demonstrating the technological feasibility of coating lipid-core nanocapsules, when lecithin is a co-surfactant. Moreover, we demonstrated the blood compatibility of those nanocapsules.

To raise our hypothesis we considered that the lipid-core nanocapsules are kinetically stable colloids (19) and showed to be a promising platform as drug delivery systems (20); additionally, we took into consideration that the spray-dried chitosan-metal microparticles are able to chemically bound ciprofloxacin by coordination with the metal complexed with the polysaccharide (16). In this way, we hypothesized that a lipid-core nanocapsule could constitute the core of a new nanoparticle having lecithin-chitosan, as coating, complexed with metals, which, in turns, could complex molecules or macromolecules having different organic functional groups containing heteroatoms such as oxygen, nitrogen, sulfur and phosphorus. The new nanoparticles were called "Metal Complex Multi-wall Nanocapsules" (MCMN).

Taking all above into consideration, our objective was to synthesize a new surface-functionalized nanoparticle by preparing lipid-core nanocapsules stabilized with lecithin-

polysorbate 80, coated with chitosan, which is complexed with iron or zinc to bind an antibody fragment. To validate our hypothesis, phenylalanine was used as ligand model to develop the nanoparticles, and the anti-electronegative LDL single-chain fragment variable [scFv anti-LDL(−)] was selected as example to demonstrate the application of the approach. To evaluate the potential contribution of the new nanoparticles to the oxidative stress, an *in vitro* lipid peroxidation assay, using liposomes as substrate, was carried out. Furthermore, to evaluate and guarantee the viability of the ligand, molecular recognition assays against native LDL (nLDL) and electronegative LDL subfraction [LDL(−)] were performed. If the tertiary structure of scFv anti-LDL(−) is intact after binding to the metal at the surface of the MCMN, the new nanoparticles would be able to distinguish native LDL and LDL(−), since this antibody fragment is specific for the latter. To validate the result, the molecular recognition was also performed using 2C7 monoclonal antibody to detect the specific binding in an enzyme linked immuno sorbent assay.

MATERIALS AND METHODS

Materials

Poly(ε-caprolactone) (PCL) (α,ω-dihydroxy functional polymer; Mn: 10,000 g mol^{-1}, Mw: 14,000 g mol^{-1}), sorbitan monostearate (Span 60®), chitosan low molar weight (Mw: 50,000–190,000 g mol^{-1}, 75–85% deacetylated polymer), zinc acetate and iron (II) chloride tetrahydrate were supplied by Sigma-Aldrich Co. Caprylic/capric triglyceride and polysorbate 80 were delivered by Delaware (Porto Alegre, Brazil). Lipoid S75 (soybean lecithin) was obtained from Lipoid (Germany). All aqueous solutions were prepared using deionized water (resistivity of 18.2 MΩ) obtained with a Millipore Direct-Q® system. Phosphate buffered saline (PBS), pH 7.4, was obtained from Laborclin (Brazil). The solvents, acetone (analytical grade) and ethanol (analytical grade), were obtained from Nuclear (Brazil). All reagents were used as received.

One-pot Synthesis of the Surface-Functionalized Metal-Complex Multi-Wall Nanocapsules (MCMN)

In a flask, poly(ε-caprolactone) (0.1 g), sorbitan monostearate (0.04 g), caprylic/capric triglyceride (0.120 g) were dissolved in acetone (25 mL) (1 h at 40°C). Then, a solution of soybean phosphatidylcholine (Lipoid S 75®) (0.03 g) in ethanol (5 mL) was added. This organic phase was poured into a round bottom flask containing polysorbate 80 (0.08 g) in water (50 mL) under magnetic stirring at room temperature. After 10 min, the round bottom flask was connected to a rotative evaporator to eliminate acetone and concentrate the turbid solution under reduced pressure (35–40°C) to a volume of 9 mL. In a separate flask, a 0.3% chitosan aqueous solution was prepared using 1% acetic acid. This chitosan solution was filtered and slowly added (1 mL) over the turbid solution under moderate magnetic stirring. After 4 h, the iron (II) chloride tetrahydrate aqueous solution or the zinc acetate aqueous solution was slowly added into the reaction medium under magnetic stirring (500 rpm) and, then, the ligand aqueous solution was added using an excess (3:1 mol/mol, ligand/metal) to passivate the nanocapsule surface and stabilize the colloids.

A variety of formulations was prepared using two different concentrations of Fe^{2+} (50 and 100 μg mL^{-1}) and four different concentrations of Zn^{2+} (10, 25, 50 and 100 μg mL^{-1}).

To develop and optimize the synthesis, phenylalanine was used as model ligand. To demonstrate the applicability of the synthesis, scFv anti-LDL(−) was used at 100 or 200 μg mL^{-1} as ligand at the surface of the MCMN.

Physicochemical Characterization of the Surface-Functionalized Metal-Complex Multi-Wall Nanocapsules (MCMN)

The pH values of the MCMN were determined using a potentiometer B474 (Micronal, Brazil). The nanocapsule aqueous suspensions were characterized with respect to their mean diameter, polydispersity index (PDI) and zeta potencial (ζ) by dynamic light scattering (DLS) and laser Doppler electrophoresis (LDE) measured at 25°C (Zetasizer® Nano ZS, Malvern Instruments Ltd., UK). Samples were previously diluted with MilliQ® water and 0.01 mol L^{-1} NaCl aqueous solution, respectively. The dilution media were filtered (0.45 μm) before analyses, but each sample was directly used without filtration or any other treatment avoiding sample selection. The measurements were carried out using three different batches for each formulation. Each analysis was carried out using 20 scans for zeta potential and ten scans for mean diameter. Mean values were obtained considering triplicate of analysis for three batches. In this way, the standard deviations were calculated by the mean values among the batches. The mean values of size distribution width were calculated by the software Dispersion Technology Software (version 4.00, 2002, Malverns Instruments ltd) using data from three different batches analyzed in triplicate ($n=3$).

The size distribution measurement was also determined by laser diffraction (LD) (Mastersizer 2000, Malvern Instruments Ltd, UK) and nanoparticle tracking analysis (NTA) (NanoSight LM10 & NTA 2.0 Analytical Software, NanoSight Ltd). The latter also provided visual information of the light scattered by the particle in solution. The video images of the light scattered by the particle in Brownian motion were followed in real-time via CCD camera. The MCMN were diluted 5,000 times and each video clip was captured over 120 s. NTA 2.0 Analytical Software

(NanoSight®) was used for calculations. All measurements were performed in triplicates.

Transmission Electron Microscopy

MCMN-Zn (25 μg mL^{-1} of zinc), MCMN-Fe (50 μg mL^{-1} of iron), and Phe-MCMN-Zn (25 μg mL^{-1} of zinc) and Phe-MCMN-Fe (50 μg mL^{-1} of iron) prepared with phenylalanine/metal at 3:1 molar ratio were diluted with water and deposited on specimen grid (Formvar Carbon support film, Electron Microscopy Sciences). Uranyl acetate solution (2%, w/v) was used as contrast agent (negatively stained). The transmission electron microscope (TEM; JEM 1200 Exll) was operating at 80 kV at the *Centro de Microscopia Eletrônica* from the Federal University of *Rio Grande do Sul* (UFRGS).

Evaluation of *In Vitro* Lipid Peroxidation

In this assay, phosphatidylcholine (Lipoid S-75) liposomes (50 mg mL^{-1}) were prepared by reverse-phase evaporation to act as substrate to lipid peroxidation. *In vitro* lipid peroxidation experiments were conducted as previously described (21) with some modifications.

The extent of lipid peroxidation was determined by the thiobarbituric acid method. The amount of lipid peroxidation was quantified by interpolating the experimental absorbance with the malondialdehyde responses obtained using the correlation curve of malondialdehyde substance reference and expressed as thiobarbituric acid reactive substances (TBARS). The curve had a correlation coefficient of 0.997, a slope of 0.165 and an intercept of −0.0055.

We prepared different controls: one positive and two negative controls. The positive control consisted of a buffered reaction medium containing 10 μL of 500 mmol L^{-1} $FeSO_4$; 10 μL of 10 mmol L^{-1} ascorbic acid and 53.6 μL of phosphatidylcholine liposomes. The negative controls were: (**1**) control of background absorbance: medium containing ascorbic acid and liposomes in buffered medium, and (**2**) control of absorbance due to the chitosan reactivity: medium containing ascorbic acid, liposomes in buffered medium added of MN formulation.

We also compared the lipid peroxidation response of $FeCl_2.4H_2O$ and zinc acetate aqueous solutions at the same concentrations of the metals in the formulations. Additionally, we also compared the Phe-MCMN-Zn and Phe-MCMN-Fe formulations with those metals free (LNC and MN). The test samples were prepared by adding 20 μL of 1 M Tris–HCl buffer, pH 7.4, in test tubes. Then, 5.86 μL of the samples [LNC, MN, Phe-MCMN-Zn (25 μg mL^{-1} of zinc) and Phe-MCMN-Fe (50 μg mL^{-1} of iron)] were added in each test tube. All formulations were diluted in the same concentration of particles per volume.

All reaction media had a final volume of 200 μL, after adding all reagents using distilled water to adjust the volume when needed. In this case, the positive control received 106.4 μL; the negative controls (**1**) and (**2**), 116.4 μL and 110.5 μL, respectively; and all other samples [LNC, MN, Phe-MCMN-Zn (25 μg mL^{-1} of zinc) and Phe-MCMN-Fe (50 μg mL^{-1} of iron)] received 100.4 μL of distilled water.

Each test sample reaction was initiated by adding, in each test tube, 10 μL of 500 mmol L^{-1} $FeSO_4$ solution, 10 μL of 10 mmol L^{-1} ascorbic acid and 53.6 μL of phosphatidylcholine liposome. All reaction media were incubated for 30 min at 37 °C. Then, 200 μL of TCA (trichloroacetic acid 12%) and of TBA (thiobarbituric acid 0.73%) were added under stirring and maintained for 30 min at 100 °C. Each reaction medium was centrifuged (15,300×*g*) for 10 min at room temperature (Sigma 1–14, SIGMA Laborzentrifugen GmbH, Germany) and analyzed by spectrophotometry at 535 nm (UV-1601 PC Spectrophotometer, Schimadzu, Japan). The experimental absorbance for the reactions of $FeCl_2.4H_2O$ and zinc acetate aqueous solutions, as well as of LNC was obtained by subtracting the absorbance observed from the absorbance of the negative control (**1**). Furthermore, the experimental absorbance for the reactions of MN, Phe-MCMN-Zn (25 μg mL^{-1} of zinc) and Phe-MCMN-Fe (50 μg mL^{-1} of iron) was obtained by subtracting the absorbance observed from the absorbance of the negative control (**2**). The solutions and formulations were prepared in triplicate batches, and one replicate of each batch was reacted with $FeSO_4$ and ascorbic acid in the presence of phosphatidylcholine liposome.

Molecular Recognition Against Native LDL and LDL(−)

Ethics Approval

The LDL subfractions were isolated from human blood, which experimental protocols were approved by the Research Ethics Committee of the Faculty of Pharmaceutical Sciences of the University of Sao Paulo.

Dynamic Light Scattering

Two subfractions of low density lipoprotein [native LDL and LDL(−)] were used in order to evaluate the selective reactivity of scFv anti-LDL(−) after complexation at the MCMN surface. Both LDL subfractions were isolated from human plasma as previously reported (22). The *in vitro* molecular recognition assay was based on the reactivity of LDL(−) with scFv anti-LDL(−)-functionalized nanocapsules. In this way, dynamic light scattering (DLS) was used to evaluate the reactivity by observing the variation of mean particle diameter and polydispersity index (PDI) as a function of the concentration of LDL(−).

The first step consisted of incubating LDL(−) or native LDL with scFv anti-LDL(−)-functionalized nanocapsules [prepared with zinc at 25 mg mL^{-1} and scFv anti-LDL(−) at 25, 50 or 100 μg mL^{-1}]. In separate flasks, 25 μL of the LDL(−) solution (361.6 μg mL^{-1}) were added of 25 μL of each formulation [scFv anti-LDL(−)-MCMN-Zn]. In parallel, the same procedure was carried out using 25 μL of the native LDL solution (690 μg mL^{-1}) and 25 μL of each formulation [scFv anti-LDL(−)-MCMN-Zn at 25, 50 or 100 μg mL^{-1}]. Using an automated pipettor, each sample was mixed thoroughly for 10× and subsequently incubated at 25 °C for 2 min prior to DLS evaluation. The mean sizes (z-average) and size distributions were calculated by the Dispersion Technology Software (version 4.00, 2002 Malverns Instruments ltd) using data from three different batches analyzed in triplicate ($n=3$).

Enzyme Linked Immuno Sorbent Assay

ELISA assays were carried out according to a previous work (23) with modifications. The 96-well plates were coated with 25 μg mL^{-1} of scFv anti-LDL(−)-MCMN-Zn or scFv anti-LDL(−) solution (positive control) at 4 °C overnight. Then, 2C7 monoclonal antibody, developed as previously described (23), was added at a concentration of 10 μg mL^{-1} and incubated for 1 h at 37 °C to recognize the LDL(−) binding to scFv anti-LDL(−)-MCMN-Zn. In parallel, an assay using nLDL was performed as negative control. A goat anti-mouse HRP (diluted 1:1,500 with 1% skim milk; Immuno Tools; Cat. N. 22339919) was added for 1 h at 37 °C. Specific binding was detected with tetramethyl benzidine (TMB) substrate for color development, and the absorbance was measured at 450 nm using a microplate reader (Apollo LB 911; Berthold Technologies). The data from two independent experiments, performed in triplicate, were analyzed using ANOVA test and all calculations were performed using GraphPad Prism software.

RESULTS AND DISCUSSION

Synthesis of the Metal-Complex Multi-wall Nanocapsules

The metal-complex multi-wall nanocapsules, represented schematically in Fig. 1, are formed by an organogel as core, poly(ε-caprolactone) as first wall, polysorbate 80 and lecithin as stabilizer system, chitosan as second wall complexed with metals (iron or zinc). We selected iron and zinc as metals in this approach because they are biocompatible and essential elements for the body (24).

The coating of lipid-core nanocapsules (LNC) with the cationic polymer (chitosan) is a critical step to reach the supramolecular structure of multi-wall nanocapsules (MN).

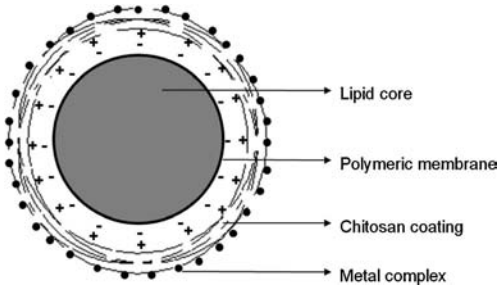

Fig. 1 Schematic representation of the MCMN structure containing iron or zinc as metal complex at the surface.

Initially, we tried unsuccessfully reacting LNC with 1% and 2% chitosan aqueous solutions. Then, better results were obtained using chitosan solutions at 0.3% and 0.5%. Chitosan at 0.3% produced better reproducible MN formulations having unimodal and nanoscopic particle size profiles (Fig. 2a). The almost superimposed granulometric profiles comparing the size distribution by volume to the size distribution by number of particles indicated a high homogeneity of the sample in particle sizes. The formation of multi-wall nanocapsules is based on the electrostatic interactions at their surface between the ammonium groups of chitosan and the negatively charge groups present in Lipoid S75 (lecithin) as impurities. The addition of the Fe^{+2} or Zn^{+2} solution into the suspension containing the multi-wall nanocapsules leads to the chitosan-metal complex formation. This complex is highly reactive, and, then, capable of combining with different molecular or macromolecular compounds.

At a first approach, the aminoacid phenylalanine was used to passivate the surface of the metal-complex multi-wall nanocapsules (MCMN). In all formulations, the aminoacid was used in excess in relation to the stoichiometry of the metal (3:1, mol/mol) to guarantee the passivation of the surface, avoiding aggregation of the nanoparticles. For Phe-MCMN-Fe, we observed unimodal distributions when 50 μg mL^{-1} iron was added with a volume-weighted mean diameter (D[4,3]) of 130 nm and polydispersity (SPAN) of 0.96 (Fig. 2b). However, when 100 μg mL^{-1} iron was used a bimodal profile was observed (Fig. 2c). As a consequence, D[4,3] was 1.10 μm with a SPAN of 1.02 for the latter. Both formulations had unimodal granulometric profiles calculated by number of particles indicating that the latter is contaminated with few micrometric particles. In this case, the results indicated that 100 μg mL^{-1} iron was in excess compared to the concentration of chitosan. This excess caused aggregation of the particles in suspension and as a consequence the microscopic contamination.

In parallel, MN added of zinc at concentrations equal or lower than 25 μg mL^{-1} followed by the addition of phenylalanine (3:1, mol/mol) showed unimodal granulometric profiles for the Phe-MCMN-Zn formed with narrow size distributions (Fig. 2d and e). Whereas, MN added of 50 μg mL^{-1} or

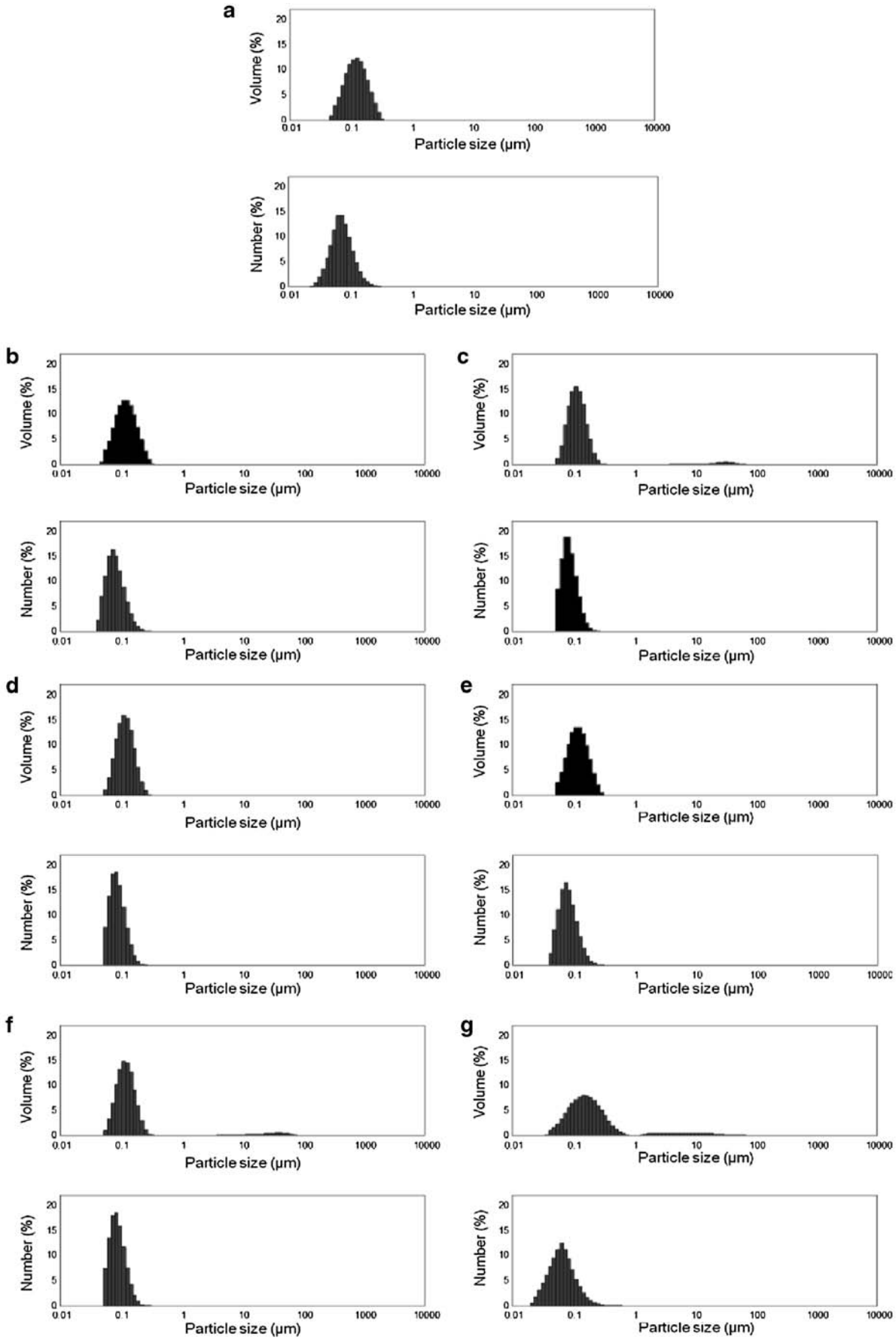
a
Volume (%)
Number (%)
Particle size (µm)
b
c
d
e
f
g
0.01
0.1
1
10
100
1000
10000
0
5
10
15
20

◀ **Fig. 2** Granulometric profiles obtained by laser diffractometry (Mastersizer 2000) of (**a**) MN, (**b**) Phe-MCMN-Fe 50 $\mu g.mL^{-1}$, (**c**) Phe-MCMN-Fe 100 $\mu g.mL^{-1}$, (**d**) Phe-MCMN-Zn 10 $\mu g.mL^{-1}$, (**e**) Phe-MCMN-Zn 25 $\mu g.mL^{-1}$, (**f**) Phe-MCMN-Zn 50 $\mu g.mL^{-1}$ and (**g**) Phe-MCMN-Zn 100 $\mu g.mL^{-1}$. Measurements were made in triplicate of batches.

100 μg mL^{-1} zinc and phenylalanine (3:1, mol/mol) favored the aggregation of the particles with consequent instability of the colloidal system (Fig. 2f and g). The D[4,3] and SPAN values for Phe-MCMN-Zn after adding zinc (10 μg mL^{-1}, 25 μg mL^{-1}, 50 μg mL^{-1} and 100 μg mL^{-1}) and phenylalanine (3:1, mol/mol) were respectively 124 nm and 0.87; 128 nm and 0.87; 1,300 nm and 1.01; and 1,420 nm and 2.65.

MCMN systems containing iron or zinc were also investigated without adding phenylalanine to surface passivation. MN samples were added exclusively of zinc or iron at the same concentrations described above. MCMN-Fe and MCMN-Zn showed polymodal granulometric profiles (Fig. 3). Thus, the metal complexed with MCMN is highly reactive easily combining with near nanocapsules causing an aggregation process, and consequently the formation of the microparticles. This process was increasingly evident as higher was the concentrations of the metals in the formulations.

Considering the high reactivity of the surface of MCMN, passivation is crucial to reach kinetically stable colloidal suspensions. Phenylalanine was essential for blocking the cross-linking of chitosan between neighboring particles. In our study, phenylalanine was added exactly 1 min after the addition of the metal ions in solution. Preliminary studies showed the lack of stability testing the addition of phenylalanine after 30 min, 15 min or 5 min.

The pre-formulation study was carried out using Laser diffractometry as technique to distinguish satisfactory the particle size profiles (unimodal at the nanoscopic scale from multimodal and/or presence of microscopic contaminants). Two formulations were selected for further analysis in order to better characterize their nanoscopic populations: Phe-MCMN-Fe prepared using iron at 50 μg mL^{-1}, and Phe-MCMN-Zn prepared using zinc at 25 μg mL^{-1}. In this way, the particle size distributions were investigated using Zetasizer® ZS and NanoSight®.

The zeta potential values varied from −10.1 ± 0.6 mV (LNC) to +8.2 ± 0.3 mV (MN) after coating the nanocapsules with chitosan. It is interesting to note that unimodal peaks of zeta potential distributions were observed for both LNC and MN formulations with reproducible profiles for different

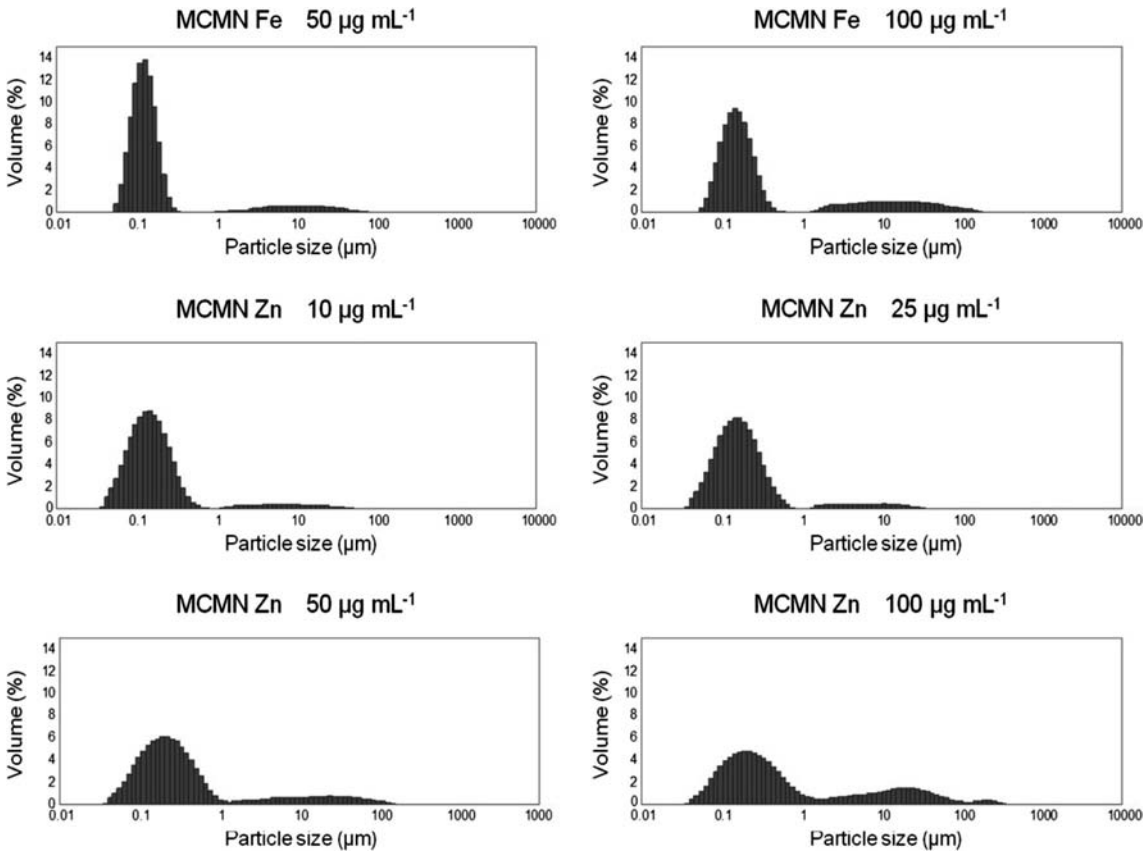

Fig. 3 Granulometric profiles by laser diffractometry (Mastersizer 2000) of MCMN-Fe and MCMN-Zn obtained with different concentrations of iron and zinc. Measurements were made in triplicate of batches ($n = 3$) without adding phenylalanine.

Table I Particle Size Distributions for LNC, MN, Phe-MCMN-Fe (50 $\mu g.mL^{-1}$) and Phe-MCMN-Zn (25 $\mu g.mL^{-1}$)

Particle diameters							
Formulation	z-average[a] (nm)	Intensity[b]		Volume		Number	
		Peak[c] (nm)	Width (nm)	Peak[c] (nm)	Width (nm)	Peak[c] (nm)	Width (nm)
LNC	123 ± 1.05	141	53	117	53	80	27
MN	133 ± 3.11*	160	70	130	71	76	29
Phe-MCMN-Fe	133 ± 0.78*	161	74	129	75	75	28
Phe-MCMN-Zn	139 ± 0.42*	159	54	128	56	77	30

[a] Mean diameter calculated by the method of cumulants and standard deviations obtained from triplicate batches ($n = 3$)

[b] Mean diameter calculated by the CONTIN algorithm

[c] Unimodal particle size distributions

*$p < 0.05$, Tukey Test

batches (Supplementary material). The results indicated the high homogeneity of coating by the cationic polymer.

Regarding the dynamic light scattering analysis (Zetasizer®), a single exponential was fit to the correlation functions (Cumulants analysis). In this way, the z-average diameters showed an increase in the mean size of the particles after coating them with chitosan (about 10 to 15 nm, $p < 0.05$) remaining constant with the addition of the metal (Table I). In addition, the particle size distributions by intensity were calculated by fitting a multiple exponential to the correlation functions (CONTIN algorithm). The results showed an increase of 20 nm after coating the LNC with the cationic polysaccharide, chitosan (Table I). The metal complexation at the nanocapsule surface had no influence on the size distributions ($p > 0.05$). The polydispersity indexes (PDI) were lower than 0.21 for all formulations corroborating that those formulations have a great homogeneity and narrow particle size distributions.

In parallel, comparing the size distributions of the formulations by intensity, volume and number (Zetasizer®), high homogeneity in particle sizes were verified since the mean diameters varied few nanometers for each formulation (Table I). The slight decrease in the mean sizes regarding the distributions by intensity, volume and number was expected considering that the intensity of scattering is proportional to d^6 from Rayleigh approximation compared to d^3 for volume and d^1 each particle interacting with the laser beam.

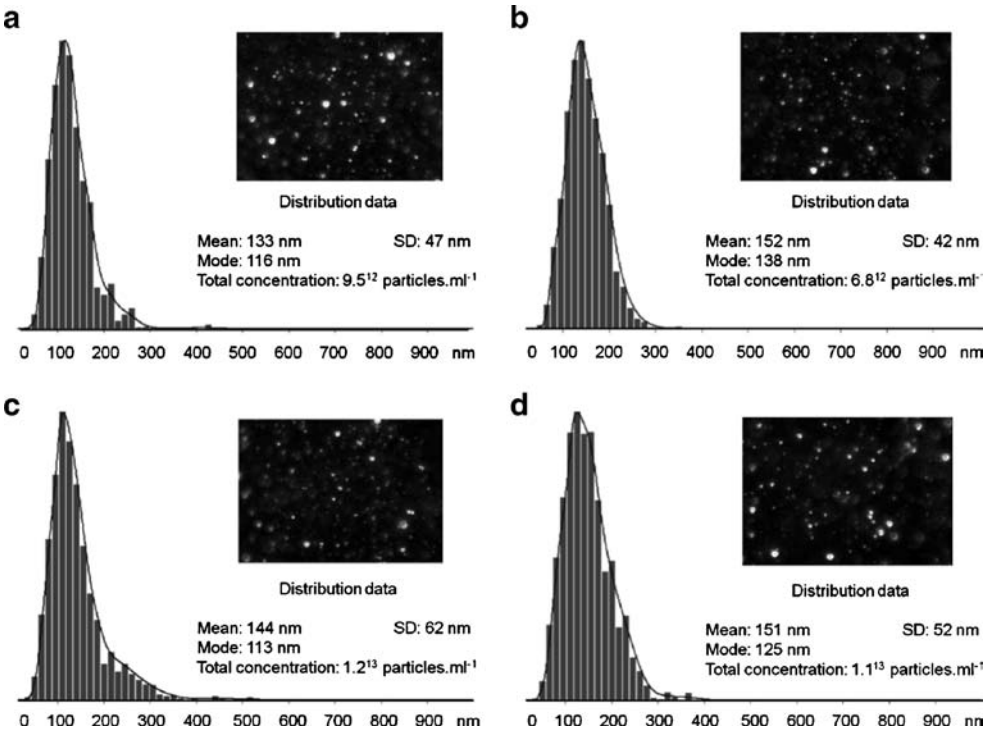

Fig. 4 Particle size distributions (nm), sample video frame (picture in black) and distribution data by NTA of LNC (**a**), MN (**b**), Phe-MCMN-Fe (50 $\mu g.mL^{-1}$) (**c**) and Phe-MCMN-Zn (25 $\mu g.mL^{-1}$) (**d**).

Nanoparticle tracking analysis (NanoSight®) can be used as an alternative to Dynamic Light Scattering (DLS) to determine the size distribution profiles of the formulations. The advantage of this technique is that the measurements are carried out by observing the light scattered from individual nanoparticles. In this way, the results are expressed in number of particles (25,26). NTA analysis is also based on the diffusional coefficient of the particles in Brownian motion relating this movement to their equivalent hydrodynamic diameters. Due to the particle-by-particle measurement basis, NTA is able to characterize better the polydisperse samples. The particle-by-particle approach allows the resolution of discrete populations of similar sizes. The formulations were diluted in water showing mean diameters of 133 nm (LNC), 152 nm (MN), 144 nm [Phe-MCMN-Fe (50 μg mL^{-1} of iron)] and 151 nm [Phe-MCMN-Zn (25 μg mL^{-1} of zinc)] (Fig. 4).

All formulations presented narrow size distributions. An increase in the particle size was observed comparing LNC to MN samples. The addition of iron (50 μg mL^{-1}) and zinc (25 μg mL^{-1}) did not affect the width of the distributions. The mean size diameters by NTA are slightly higher than the values obtained by Zetasizer® analysis. The difference could be attributed to the different particle counts between each technique (26). Spectroscopic analysis (Fourier transform infrared and nuclear magnetic resonance) carried out to elucidate the structure of the nanocapsules did not show any peak relative to chitosan (data not shown). The results can be explained by the lack of sensitivity of those techniques considering the small mass of chitosan in our formulations compared to the mass of the other constituents. The mass of chitosan is distributed at the surface of the nanocapsules causing an increase about 10 to 20 nm (cumulants or CONTIN) in their

Table II Lipid Peroxidation Expressed as Thiobarbituric Acid Reactive Substances (TBARS) for the Formulations (LNC, MN, Phe-MCMN-Fe and Phe-MCMN-Zn) and the Iron and Zinc Solutions (Fe^{2+} and Zn^{2+})

Formulations	Lipid peroxidation* (nmols TBARS mL^{-1})
Positive control	12.9 ± 0.1^{a}
Fe^{2+} solution	15.2 ± 1.3^{a}
Zn^{2+} solution	12.7 ± 0.8^{a}
LNC	5.1 ± 2.1^{b}
MN	6.9 ± 0.9 [6.6 ± 0.9]^{b}
Phe-MCMN-Fe	8.0 ± 0.8 [7.6 ± 0.5]^{b}
Phe-MCMN-Zn	7.3 ± 0.6 [6.9 ± 0.6]^{b}

*Values in brackets calculated by discounting the background absorbance generated by the chitosan reactivity

Different letters indicate statistically different values ($p < 0.05$, Tukey test)

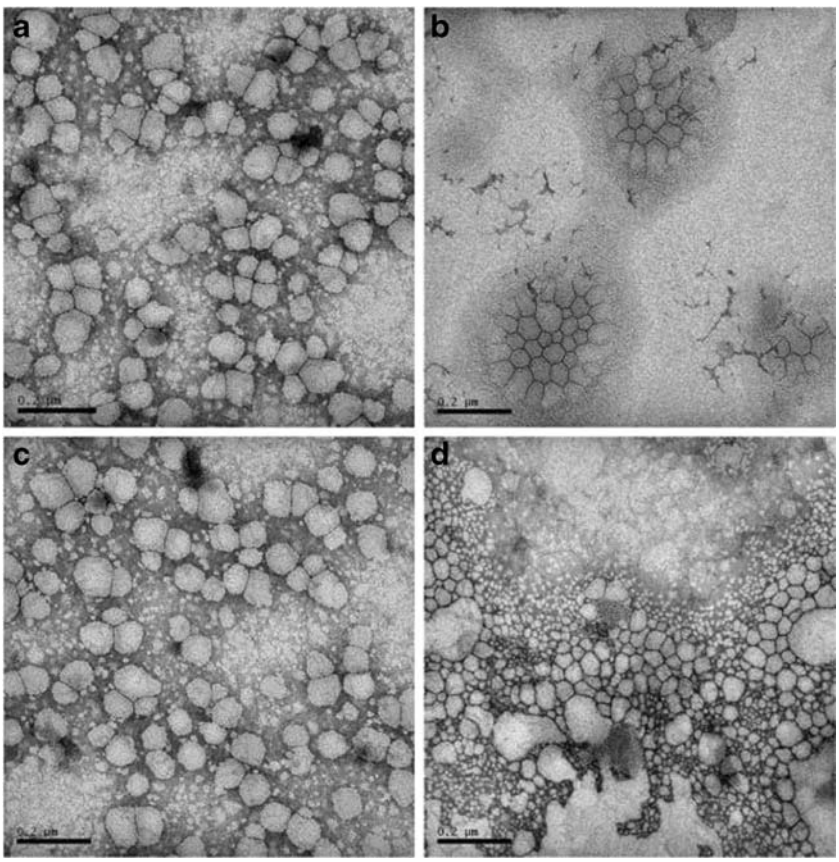

Fig. 5 Photomicrographs obtained by TEM of Phe-MCMN-Fe (**a**) and MCMN-Fe (**b**), and of Phe-MCMN-Zn (**c**) and MCMN-Zn (**d**) (bar = 200 nm).

average diameters, as well as an inversion in the zeta potential from negative to positive.

Images obtained by TEM for MCMN-Fe and Phe-MCMN-Fe at 50 μg mL^{-1} of iron and for MCMN-Zn and Phe-MCMN-Zn at 25 μg mL^{-1} of zinc showed the influence of phenylalanine in avoiding aggregation. Phe-MCMN-Fe and Phe-MCMN-Zn had particles spherically shaped (Fig 5a and c), while MCMN-Fe and MCMN-Zn showed agglomerates (Fig 5b and d). The images illustrate the results obtained by Laser diffractometry. The Phe-MCMN-Fe and Phe-MCMN-Zn had similar particle mean diameters to those determined by DLS and NTA (below 200 nm).

Different mechanisms have being proposed for the metal-chitosan complex. Zimmermann and co-workers (27) have proposed a hexacoordinate complex for iron-crosslinked chitosan and Tang and Hon (28) have considered a tetrahedral coordination as plausible mechanisms for the zinc-chitosan complex. We could envisage that similar mechanisms could occur to form Phe-MCMN-Fe and Phe-MCMN-Zn considering the metal complexation with the nitrogen atoms from the chitosan portion and the oxygen atoms from the carbonyl moieties of Phe.

In vitro Lipid Peroxidation

In vitro lipid peroxidation was investigated to determine the applicability of the new carriers specially the MCMN prepared with iron, since the nanoparticle could act as potential oxidant enhancing the oxidative stress and, therefore, being inadequate for medical purposes. Oxidative processes are related to the occurrence of a variety of changes in biological and biochemical steps at the cellular level (29). The presence of antioxidants in pharmaceutical dosage forms, such as nanoparticles, helps to avoid the incidence of these events (29,30). Tests assessing lipid peroxidation can be used to evaluate the *in vitro* occurrence of oxidative processes (21,31). In this study, we determined the extent of lipid peroxidation by the thiobarbituric acid method using liposomes as substrate (Table II).

The experimental absorbances obtained for Fe^{2+} and Zn^{2+} solutions and LNC were subtracted from the absorbance of the negative control (**1**) (0.51±0.04 nmol TBARS mL^{-1}). Likewise, the experimental absorbances obtained for MN, Phe-MCMN-Zn and Phe-MCMN-Fe were subtracted from the negative control (**2**) (0.49±0.06 nmol TBARS mL^{-1}).

The measurements are based on the presence of a secondary product from the oxidation of polyunsaturated fatty acids, known as malondialdehyde (MDA), and its complexation with

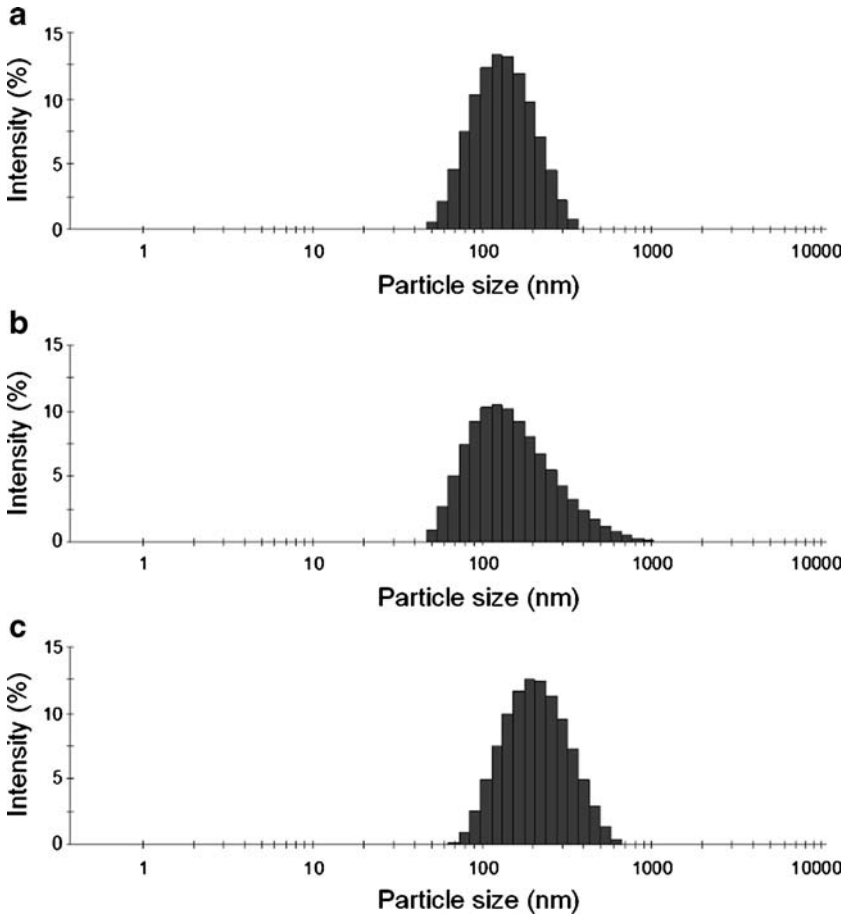

Fig. 6 Particle size distributions by dynamic light scattering (Zetasizer® ZS) (**a**) MN, (**b**) scFv anti-LDL(−)-MCMN-Zn (at 25 μg.mL^{-1} of zinc and 100 μg.mL^{-1} of scFv), (**c**) scFv anti-LDL(−)-MCMN-Zn (at 25 μg.mL^{-1} of zinc and 200 μg.mL^{-1} of scFv).

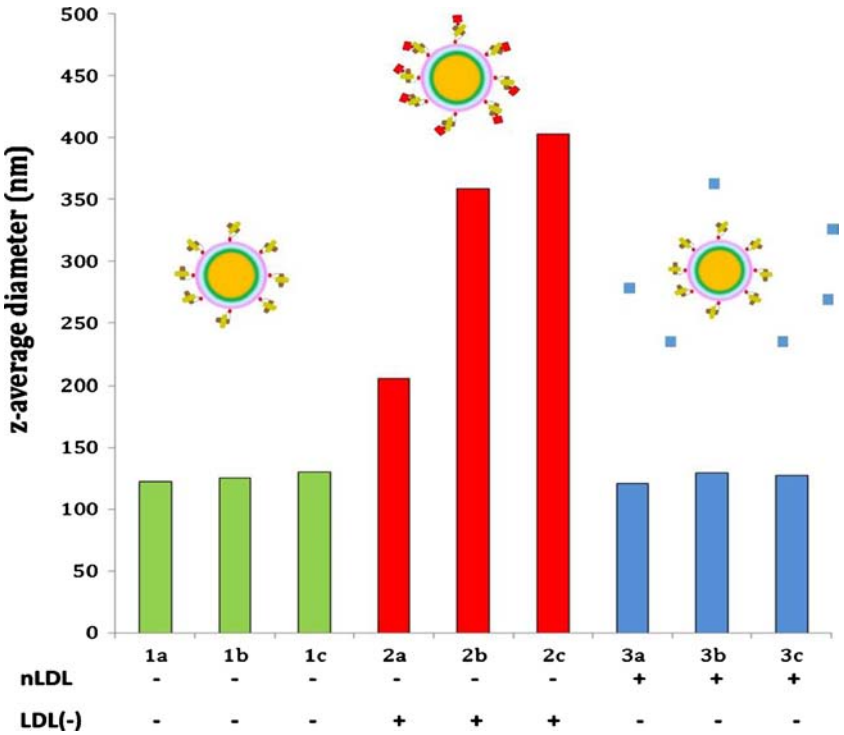

Fig. 7 Mean particle diameter (z-average) by dynamic light scattering (Zetasizer® ZS) of scFv anti-LDL(−)-MCMN-Zn [prepared with zinc at 25 mg mL^{-1} and scFv anti-LDL(−) at 25 μg mL^{-1} (**a**), 50 μg mL^{-1} (**b**) or 100 μg mL^{-1} (**c**)] after no addition of LDL(−) or nLDL (**1**), after addition of LDL(−) (**2**) and after addition of nLDL (**3**).

the nucleophile group thiobarbituric acid (TBA). The reaction promotes the formation of a chromophore with high molar absorptivity in the visible spectrum (21,32). The results showed that the Fe^{2+} and Zn^{2+} solutions had similar values to the positive control (12.9±0.1 TBARS mL^{-1}). However, the Phe-MCMN-Zn and Phe-MCMN-Fe showed lower values of lipid peroxidation in relation to the respective Fe^{2+} and Zn^{2+} solutions ($p<0.05$). An important observation is that the extent of lipid peroxidation caused by the formulations containing metals (Phe-MCMN-Zn and Phe-MCMN-Fe) was similar to that determined for LNC and MN, in which the metals are not present ($p>0.05$), indicating that iron and zinc were not free in solution but complexed with the nanocapsules. The formulations decreased the ascorbyl radical formation and thereby limited the peroxidation of the substrate (liposomes). Thus, the results suggested that Phe-MCMN-Fe and Phe-MCMN-Zn are not potential formulation to enhance the oxidative stress.

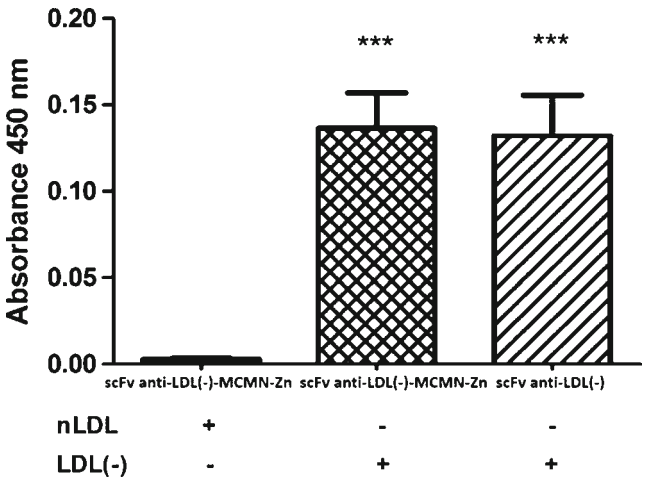

Fig. 8 Evaluation of the specificity of scFv anti-LDL(−)-MCMN-Zn to LDL(−) by ELISA. LDL(−) or nLDL were added at a concentration of 10 μg/mL to 96-well microplate coated with 25 μg.mL^{-1} of scFv anti-LDL(−)-MCMN-Zn or scFv anti-LDL(−). A goat anti-mouse HRP was diluted 1:1,500 and incubated for 1 h. TMB was used as substrate for color development and the absorbance was measured at 450 nm. The results of two independent experiments, performed in triplicate, are expressed as the means ± SD ***$p<0.001$ compared with control [scFv anti-LDL(−)-MCMN-Zn + nLDL]; ANOVA followed by the Tukey-Kramer test.

Synthesis of scFv Anti-LDL(−)-Functionalized Nanocapsules

The *in vitro* lipid peroxidation assay gave us evidence of possible applications of these new nanocapsules in therapeutics. However, considering the possibility of *in vivo* release of iron after i.v. administration in further investigations, we firstly selected the zinc, as metal, specifically to synthetize the scFv anti-LDL(−) surface functionalized nanocapsules, since the future application of those nanoparticles in an atherosclerosis experimental model could be compromised by the potential iron release.

Anti-electronegative LDL single-chain fragment variable [scFv anti-LDL(−)], expressed in *P. pastoris* (23), was added just after the addition of zinc acetate solution in the MN formulation. The recombinant antibody fragment contains

the complete binding site to the [LDL(−)] antigen. Furthermore, the C-terminal portion of the protein has an insertion of six histidine residues (hexahistidine) which can specifically bind to zinc at the MCMN-Zn surface.

MCMN-Zn samples were added of two different concentrations of scFv anti-LDL(−) (Fig. 6). The mean particle diameters (z-average) and PDI were 146 nm and 0.16 after adding 100 μg mL^{-1} of scFv anti-LDL(−), and 197 nm and 0.25 after adding 200 μg mL^{-1} of scFv anti-LDL(−). For both formulations, we observed an increase in the mean particle size as compared to MN (133 nm and 0.12). For each formulation, the narrow peak and the absence of secondary peaks in the size distribution profiles suggested the effective binding of the antibody fragments to the nanoparticle surfaces.

Molecular Recognition

Once formed, the complex scFv anti-LDL(−)-MCMN-Zn should maintain the ability to bind with LDL(−). Thus, *in vitro* tests were carried out comparing the reactivity of LDL(−) to native LDL with scFv anti-LDL(−)-MCMN-Zn.

The mean particle size of 22 nm was previously determined for LDL(−) (33,34). Therefore, because LDL(−) is highly specific to scFv anti-LDL(−) our strategy was based on the increase in the mean particles size of the colloids after reacting LDL(−) with scFv anti-LDL(−)-MCMN-Zn (positive recognition). Because of the lack of specificity of native LDL for scFv anti-LDL(−)-MCMN-Zn, no size variation was expected to be observed (negative recognition). To verify this hypothesis, we assay scFv anti-LDL(−)-MCMN-Zn [prepared with zinc at 25 mg mL^{-1} and scFv anti-LDL(−) at 25, 50 or 100 μg mL^{-1}] with native LDL and LDL(−) (Fig. 7).

In the recognition assay, the size variation (DLS) was compared to the initial particle mean sizes (Fig. 7, 1a–c). The particle mean sizes did not vary with the increase in the scFv concentration in the formulation. Continuing our study, the scFv anti-LDL(−)-MCMN-Zn added of native LDL or LDL(−) showed significant ($p<0.05$) different mean particle diameters (z-average) (Fig. 7, 2a–c and 3a–c). Moreover, scFv anti-LDL(−)-MCMN-Zn added of LDL(−) showed increased mean particle diameters ($p<0.05$) as a function of the concentration of scFv anti-LDL(−) in the formulation. After adding LDL(−), the mean particle diameter and PDI for the complex LDL(−)-scFv anti-LDL(−)-MCMN-Zn (prepared at 100 μg mL^{-1} of scFv) were 403 nm and 0.26, while for the colloidal solution of scFv anti-LDL(−)-MCMN-Zn added of native LDL those values were 127 nm and 0.18, respectively. On the contrary, we observe that all reactions carried out with scFv anti-LDL(−)-MCMN-Zn added of native LDL showed similar particle sizes ($p>0.05$) (Fig. 7, 3a–c) due to the lack of receptor in native LDL for a specific binding with scFv anti-LDL(−). Our hypothesis was validated and the results indicated the maintenance of reactivity for scFv anti-LDL(−)-MCMN-Zn added of LDL(−).

To verify quantitatively the reactivity, we performed an ELISA assay in order to compare the reactivity of scFv anti-LDL(−) to the reactivity of scFv anti-LDL(−)-MCMN-Zn with LDL(−) (Fig. 8). The statistical analysis demonstrated that scFv anti-LDL(−)-MCMN-Zn added of LDL(−) had similar reactivity and specificity to scFv anti-LDL(−) added of LDL(−). On the other hand, the reactivity of scFv anti-LDL(−)-MCMN-Zn with LDL(−) was statistically significant higher ($p<0.001$) compared to its reactivity with native LDL. The results showed that either reactivity or specificity of the scFv were preserved after its binding to the MCMN-Zn surface.

The results open the possibility of applying this new strategy as an interesting tool to bind diverse molecules or macromolecules at the nanocapsule surface envisaging a broad application for those new nanoparticles, including active drug targeting or new theranostics. The new nanocapsules could be administered by i.v., nasal, pulmonary and oral routes.

CONCLUSIONS

We proposed a new strategy to functionalize the surface of nanoparticles. The new metal-complex multiwall nanocapsules are innovative considering the one-pot synthesis of a completely biodegradable structure. The diverse response of scFv anti-LDL(−)-functionalized nanocapsules after adding either LDL(−) or native LDL indicate the maintenance of the active site of the fragment after reacting with the metal at the MCMN surface. Furthermore, the reactivity and the specificity of scFv anti-LDL(−)-MCMN-Zn in recognizing LDL(−) was unequivocally demonstrated. The new approach to bind ligands at the surface of biodegradable polymeric nanoparticles did not affect the native conformation or the active site of the antibody fragment. The performance of scFv anti-LDL(−)-MCMN-Zn makes this supramolecular structure interesting for applications in nanomedicine. Furthermore, the synthetic approach is a solvent free process of surface decoration with no need of further purification of the product. Finally, the new strategy is an interesting tool to bind diverse molecules or macromolecules at the nanoparticle surface envisaging a broad use for those new nanoparticles in Pharmaceutical Nanotechnology.

ACKNOWLEDGMENTS AND DISCLOSURES

EAB thanks CAPES/Brazil for his fellowship. The authors thank PRONEX e PRONEM FAPERGS/CNPq, FAPESP, INCT-IF/CNPq, CNPq/Brasilia/Brazil, Universal CNPq/MCTI and Rede Nanotecnologia Farmaceutica CAPES (Brazil) for grant financial supports.

REFERENCES

1. Haley B, Frenkel E. Nanoparticles for drug delivery in cancer treatment. Urol Oncol-Semin Ori. 2008;26:57–64.
2. Wang M, Thanou M. Targeting nanoparticles to cancer. Pharmacol Res. 2010;62:90–9.
3. Segala K, Dutra RL, de Oliveira EN, Rossi LM, Matos JR, Paula MMS, *et al.* Characterization of poly-{trans-RuCl2(vpy)(4)-styrene-4-vinylpyridine} impregnated with silver nanoparticles in non aqueous medium. J Braz Chem Soc. 2006;17:1679–82.
4. Byrne JD, Betancourt T, Brannon-Peppas L. Active targeting schemes for nanoparticle systems in cancer therapeutics. Adv Drug Deliv Rev. 2008;60:1615–26.
5. Huang JT, Hou SY, Fang SB, Yu HW, Lee HC, Yang CZ. Development of a biochip using antibody-coated gold nanoparticles to detect specific bioparticles. J Ind Microbiol Biotechnol. 2008;35:1377–85.
6. Betancourt T, Byrne JD, Sunaryo N, Crowder SW, Kadapakkam M, Patel S, *et al.* PEGylation strategies for active targeting of PLA/PLGA nanoparticles. J Biomed Mater Res A. 2009;91A:263–76.
7. Guan XP, Quan DP, Liao KR, Wang T, Xiang P, Mai KC. Preparation and characterization of cationic chitosan-modified poly(D, L-lactide-co-glycolide) copolymer nanospheres as DNA carriers. J Biomater Appl. 2008;22:353–71.
8. Bernardi A, Zilberstein A, Jager E, Campos MM, Morrone FB, Calixto JB, *et al.* Effects of indomethacin-loaded nanocapsules in experimental models of inflammation in rats. Br J Pharmacol. 2009;158:1104–11.
9. Zalipsky S, Wang L, Ding Z, Luo B. Nanoparticle comprises nucleic acid and composition formed by combining cationic polymer conjugate covalently linked to hydrophilic polymer and unconjugated cationic polymer, where nucleic acid and cationic polymer form non-covalent complex. US Patent No. WO2011011631-A2, 2011.
10. Zhang L, Swift J, Butts SA, Dmochowski IJ. INOR 631-protein-templated gold nanoparticle synthesis and assembly. Abstr Pap Am Chem Soc. 2008;236:631–INOR.
11. Cheng XH, Chen G, Rodriguez WR. Micro- and nanotechnology for viral detection. Anal Bioanal Chem. 2009;393:487–501.
12. Li D, Teoh WY, Gooding JJ, Selomulya C, Amal R. Functionalization strategies for protease immobilization on magnetic nanoparticles. Adv Funct Mater. 2010;20:1767–77.
13. Letchford K, Liggins R, Wasan KM, Burt H. In vitro human plasma distribution of nanoparticulate paclitaxel is dependent on the physicochemical properties of poly(ethylene glycol)-block-poly(caprolactone) nanoparticles. Eur J Pharm Biopharm. 2009;71:196–206.
14. Jager E, Venturini CG, Poletto FS, Colome LM, Pohlmann JPU, Bernardi A, *et al.* Sustained release from lipid-core nanocapsules by varying the core viscosity and the particle surface area. J Biomed Nanotechnol. 2009;5:130–40.
15. Jornada DS, Fiel LA, Bueno K, Gerent JF, Petzhold CL, Beck RCR, *et al.* Lipid-core nanocapsules: mechanism of self-assembly, control of size and loading capacity. Soft Matter. 2012;8:6646–55.
16. Reynaud F, Tsapis N, Deyme M, Vasconcelos TG, Gueutin C, Guterres SS, *et al.* Spray-dried chitosan-metal microparticles for ciprofloxacin adsorption: kinetic and equilibrium studies. Soft Matter. 2011;7:7304–12.
17. Rodrigues CA, Reynaud F, Stadler E, Drago V. Preparation, characterization, and chromatography properties of chitin modified with FeCl3. J Liq Chromatogr Relat Technol. 1999;22:761–9.
18. Bender EA, Adorne MD, Colome LM, Abdalla DSP, Guterres SS, Pohlmann AR. Hemocompatibility of poly(epsilon-caprolactone) lipid-core nanocapsules stabilized with polysorbate 80-lecithin and uncoated or coated with chitosan. Int J Pharm. 2012;426:271–9.
19. Fiel LA, Adorne MD, Guterres SS, Netz PA, Pohlmann AR. Variable temperature multiple light scattering analysis to determine the enthalpic term of a reversible agglomeration in submicrometric colloidal formulations: a quick quantitative comparison of the relative physical stability. Colloid Surface A. 2013;431:93–104.
20. Pohlmann AR, Fonseca FN, Paese K, Detoni CB, Coradini K, Beck RCR, *et al.* Poly(epsilon-caprolactone) microcapsules and nanocapsules in drug delivery. Expert Opin Drug Del. 2013;10:623–38.
21. Schaffazick SR, Pohlmann AR, de Cordova CAS, Creczynski-Pasa TB, Guterres SS. Protective properties of melatonin-loaded nanoparticles against lipid peroxidation. Int J Pharm. 2005;289:209–13.
22. Faulin TDS, de Sena KCM, Telles AER, Grosso DM, Faulin EJB, Abdalla DSP. Validation of a novel ELISA for measurement of electronegative low-density lipoprotein. Clin Chem Lab Med. 2008;46:1769–75.
23. Kazuma SM, Cavalcante MF, Telles AER, Maranhão AQ, Abdalla DSP. Cloning and expression of an anti-LDL(−) single chain variable fragment, and its inhibitory effect on experimental atherosclerosis. mABs. 2013;5:763–75.
24. Ouedraogo HZ, Traore T, Zeba AN, Dramaix-Wilmet M, Hennart P, Donnen P. Effect of an improved local ingredient-based complementary food fortified or not with iron and selected multiple micronutrients on Hb concentration. Public Health Nutr. 2010;13:1923–30.
25. Le TT, Saveyn P, Hoa HD, Van der Meeren P. Determination of heat-induced effects on the particle size distribution of casein micelles by dynamic light scattering and nanoparticle tracking analysis. Int Dairy J. 2008;18:1090–6.
26. Filipe V, Hawe A, Jiskoot W. Critical evaluation of Nanoparticle Tracking Analysis (NTA) by NanoSight for the measurement of nanoparticles and protein aggregates. Pharm Res. 2010;27:796–810.
27. Zimmermann AC, Mecabô A, Fagundes T, Rodrigues CA. Adsorption of Cr(VI) using Fe-crosslinked chitosan complex (Ch-Fe). J Hazard Mater. 2010;179:192–6.
28. Tang LG, Hon DNS. Chelation of chitosan derivatives with zinc ions. II. Association complexes of Zn^{2+} onto *O*,*N*-carboxymethyl chitosan. J Appl Polym Sci. 2001;79:1476–85.
29. Byun Y, Hwang JB, Bang SH, Darby D, Cooksey K, Dawson PL, *et al.* Formulation and characterization of alpha-tocopherol loaded poly epsilon-caprolactone (PCL) nanoparticles. Food Sci Technol–Leb. 2011;44:24–8.
30. Amorim CD, Couto AG, Netz DJA, de Freitas RA, Bresolin TMB. Antioxidant idebenone-loaded nanoparticles based on chitosan and N-carboxymethylchitosan. Nanomed Nanotech Biol Med. 2010;6:745–52.
31. Abdalla DSP, de Sena KCM. Lipid peroxidation biomarkers in atherosclerosis. Rev Nutr. 2008;21:749–56.
32. Janero DR. Malondialdehyde and thiobarbituric acid-reactivity as diagnostic indexes of lipid-peroxidation and peroxidative tissue-injury. Free Radic Biol Med. 1990;9:515–40.
33. Prassl R, Laggner P. Molecular structure of low density lipoprotein: current status and future challenges. Eur Biophys J. 2009;38:145–58.
34. Faulin TDS, de Sena-Evangelista KCM, Pacheco DB, Augusto EM, Abdalla DSP. Development of immunoassays for anti-electronegative LDL autoantibodies and immune complexes. Clin Chim Acta. 2012;413:291–7.